

Stabilizing Copper by a Reconstruction-Resistant Atomic Cu–O–Si Interface for Electrochemical CO₂ Reduction

Xin Tan,¹ Kaian Sun,¹ Zewen Zhuang,¹ Botao Hu, Yu Zhang, Qinggang Liu, Chang He, Zhiyuan Xu, Chang Chen, Hai Xiao, and Chen Chen^{*}



Cite This: *J. Am. Chem. Soc.* 2023, 145, 8656–8664



Read Online

ACCESS |

Metrics & More

Article Recommendations

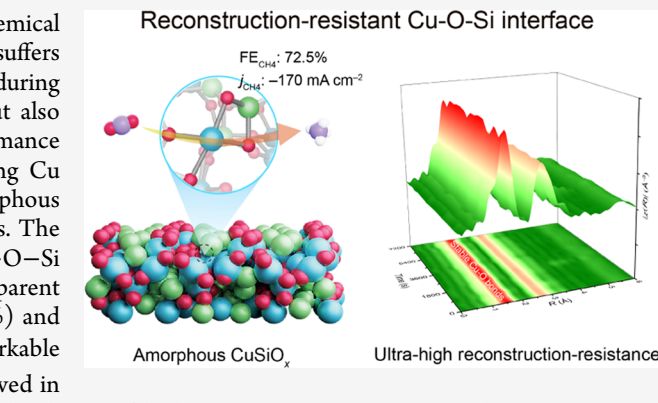
Supporting Information

ABSTRACT: Copper (Cu), a promising catalyst for electrochemical CO₂ reduction (CO₂R) to multi-electron reduction products, suffers from an unavoidable and uncontrollable reconstruction process during the reaction, which not only may lead to catalyst deactivation but also brings great challenges to the exploration of the structure–performance relationship. Herein, we present an efficient strategy for stabilizing Cu with silica and synthesize reconstruction-resistant CuSiO_x amorphous nanotube catalysts with abundant atomic Cu–O–Si interfacial sites. The strong interfacial interaction between Cu and silica makes the Cu–O–Si interfacial sites ultrastable in the CO₂R reaction without any apparent reconstruction, thus exhibiting high CO₂-to-CH₄ selectivity (72.5%) and stability (FE_{CH₄} remains above 60% after 12 h of test). A remarkable CO₂-to-CH₄ conversion rate of 0.22 μmol cm⁻² s⁻¹ was also achieved in a flow cell device. This work provides a very promising route for the design of highly active and stable Cu-based CO₂R catalysts.

INTRODUCTION

The renewable-energy-powered electrochemical CO₂ reduction (CO₂R) to value-added products is a promising solution for reducing the atmospheric CO₂ concentration and achieving sustainable carbon recycling.^{1–6} Among the electrocatalysts for CO₂R, copper (Cu)-based materials are unique candidates for the multi-electron reduction products (such as methane, ethylene, ethanol, *etc.*) with appreciable activity.^{7–9} However, the products of Cu-catalyzed CO₂R are widely distributed, and the activity and selectivity for a specific product are still unsatisfactory. Therefore, it is of utmost significance to improve the catalytic activity, selectivity, and stability of Cu-based catalysts for their industrial applications.^{10,11}

Uncontrollable reconstruction in the electrochemical CO₂R reaction is the main problem for Cu-based materials,^{12,13} which makes some predesigned active site structures hardly maintainable during the electrochemical process, resulting in reduced catalytic activity or even complete deactivation of catalysts. Although some reconstructed Cu (r-Cu) catalysts, such as oxide-derived Cu (OD-Cu),^{14,15} demonstrated high performance in CO₂R reaction, the real active structures of r-Cu and the relationship between structure and performance have been shrouded in mystery due to the uncontrollable and sophisticated reconstruction process.^{16–18} Several avenues (such as introducing a second metal, carbon confinement, *etc.*) have previously been employed to stabilize Cu catalysts and resist the reconstruction.^{19–22} At present, there are still some limitations, such as unsatisfactory activity and unabiding



stability, and thus the requirements for practical application cannot be met. Hence, the design and synthesis of Cu-based electrocatalysts with high resistance to reconstruction play a vital role in increasing their long-lasting activity and selectivity and revealing their structure–performance relationship in CO₂R reaction.

Cu/SiO₂ catalysts are widely used in thermocatalytic hydrogenation reactions, in which SiO₂ acts as a support to stabilize Cu species and promote their activity through strong metal–support interactions.^{23–25} This bears the important and to-date untested hypothesis of whether this strong interfacial interaction can be used to stabilize Cu against electrochemical reconstruction during the CO₂R process. Herein, we designed an amorphous CuSiO_x catalyst in which Cu species are uniformly dispersed in the silica matrix accompanied with abundant atomic Cu–O–Si interfacial sites. The unique atomic interfacial sites endow CuSiO_x catalyst with high CO₂-to-CH₄ selectivity (72.5%) and stability (FE_{CH₄} remains above 60% after 12 h of test). *In situ* X-ray absorption spectrum (XAS) studies revealed that the catalyst is ultrastable

Received: February 14, 2023

Published: April 8, 2023



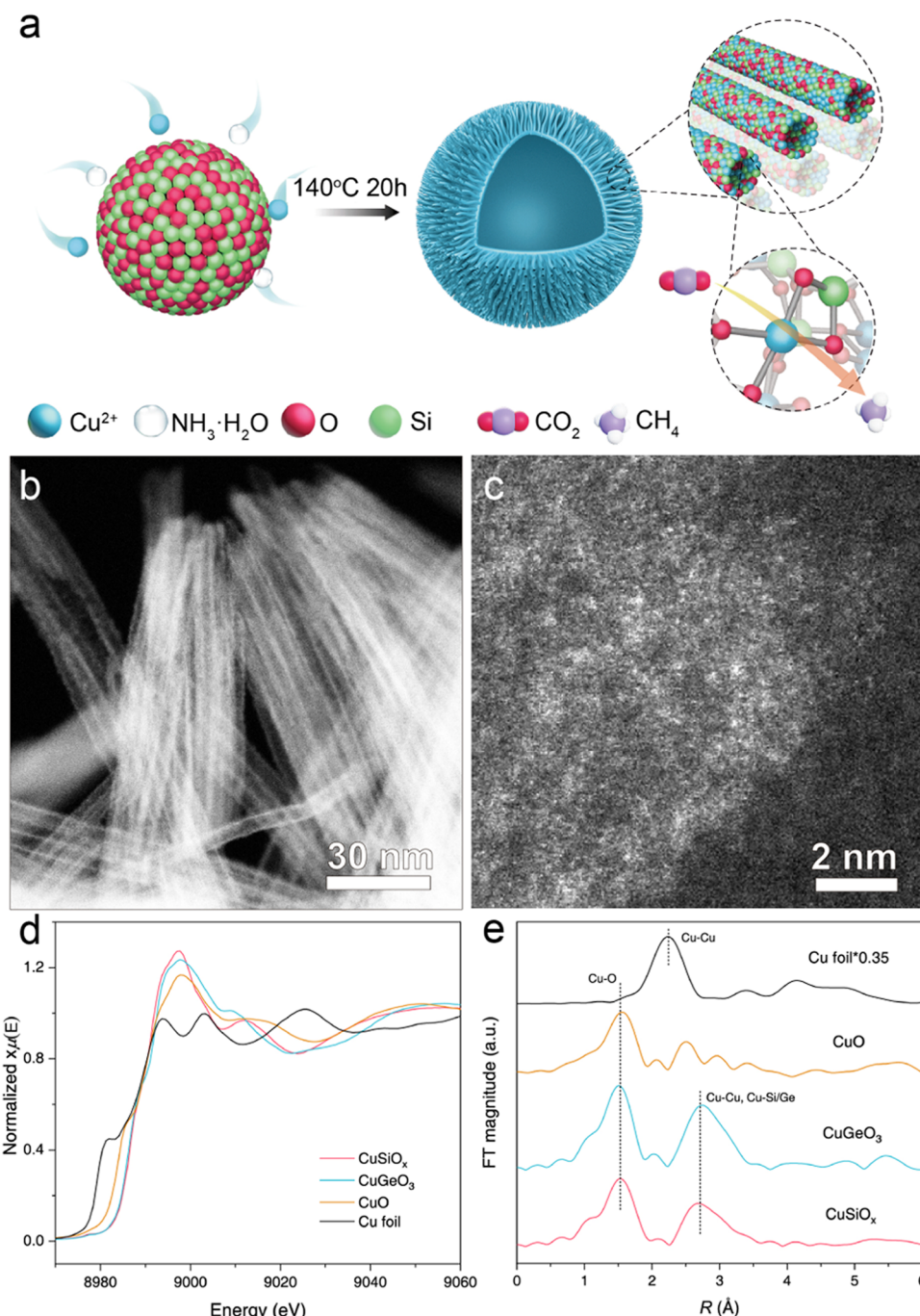


Figure 1. Morphological and fine structural characterization. (a) Schematic illustration of the CuSiO_x synthetic process. (b, c) AC-HAADF-STEM images of CuSiO_x . Cu K-edge (d) XANES and (e) FT-EXAFS spectra of the as-synthesized samples.

and reconstruction-resistant during the electrochemical CO_2R process, with no apparent changes in the structure of active Cu species. Density functional theory calculations suggested that the interface with silica could increase the Cu–O bond strength, thus improving the reconstruction resistance of Cu species. And the Cu–O–Si interfacial sites prefer to generate methane through a $^*\text{CO}$ protonation to $^*\text{COH}$ pathway rather than hydrogen evolution or C–C coupling in terms of reaction thermodynamics.

RESULTS AND DISCUSSION

Material Synthesis and Characterization. The CuSiO_x catalyst was synthesized by hydrothermal method using

presynthesized SiO_2 nanospheres as templates (Figures 1a and S1). X-ray diffraction (XRD) patterns (Figure S2a) showed a weak diffraction peak intensity of CuSiO_x , indicating its amorphous characteristic. Scanning electron microscopy (SEM) and transmission electron microscopy (TEM) images showed that CuSiO_x exhibited a hollow nanosphere morphology (~ 650 nm in diameter) with radially arranged nanotubes (~ 5.5 nm in diameter) on the surface (Figures 1b and S2b,c). The AC-HAADF-STEM images (Figures 1c and S2d) and energy-dispersive X-ray (EDX) element mappings (Figure S2e–h) confirmed that Cu atoms were uniformly distributed on the nanotubes, forming abundant atomic Cu–O–Si interfacial sites. Brunauer–Emmett–Teller (BET) results

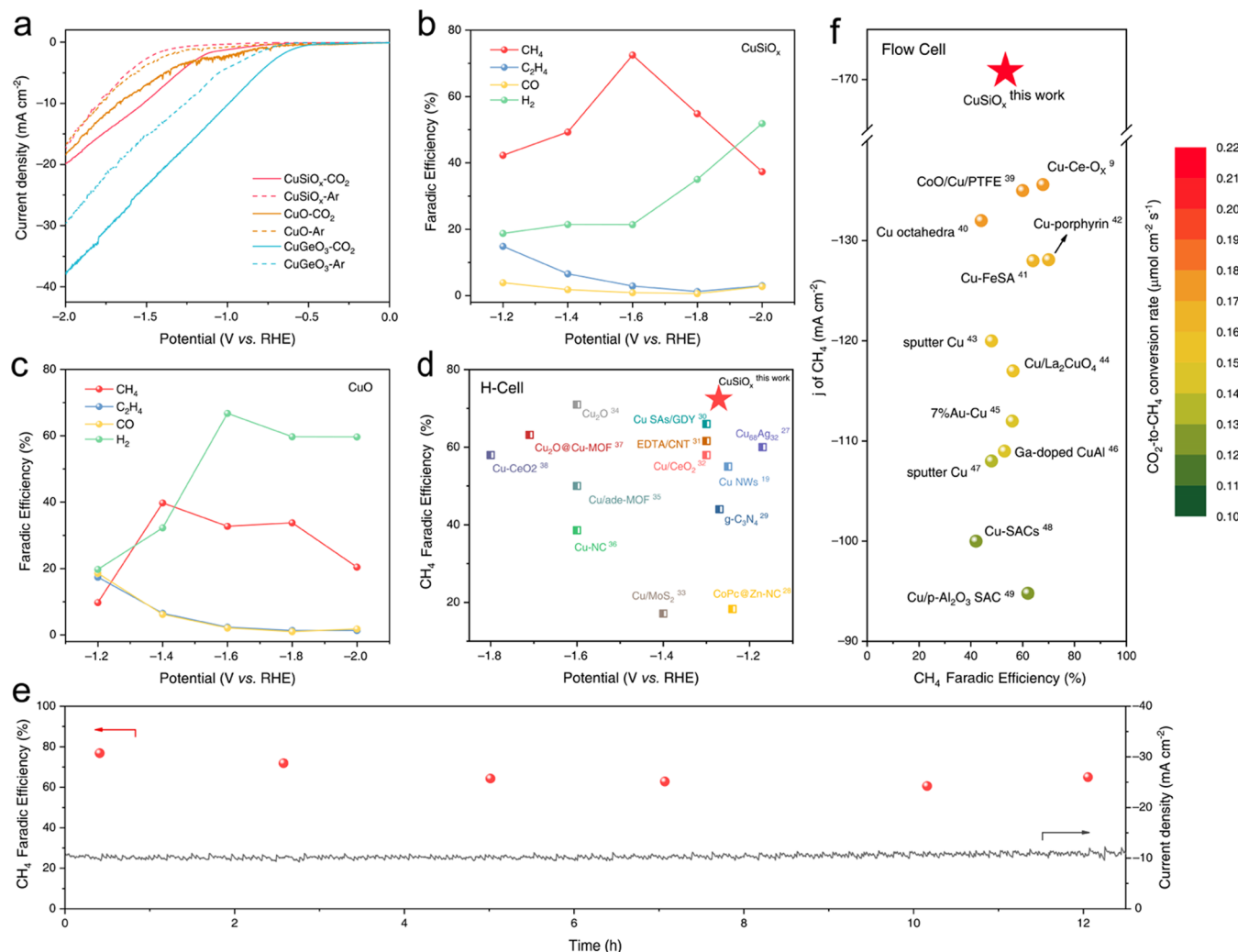


Figure 2. Electrochemical CO₂R performance. (a) LSV curves of CuSiO_x, CuGeO₃, and CuO purged with CO₂ or Ar. (b, c) FEs of CO₂R products at different potentials. (d) FE_{CH₄} of CuSiO_x in comparison with other reported catalysts after iR (refs 19, 27–38). (e) Time-dependent total current density and FE_{CH₄} for CuSiO_x recorded at -1.6 V vs RHE for 12 h. (f) Comparison of this work with previous studies on the electrocatalytic CO₂-to-CH₄ reaction in a flow cell device (refs 9, 39–49).

showed that the specific surface area of CuSiO_x was as high as 478.05 m²/g (Figure S4). To better understand the stabilization effect of Si, we replaced Si with Ge, the element in the same main group, to synthesize CuGeO₃ comparative catalyst (Figure S5). For comparison, commercial CuO was also studied (Figure S6). XAS was further performed to investigate the fine structure of the catalysts. The X-ray absorption near-edge structure (XANES) of Cu K-edge is shown in Figure 1d. The absorption threshold position of CuSiO_x was almost the same as that of CuGeO₃, indicating the similar oxidation state of +2. The Fourier transforms of the extended X-ray absorption fine structure (EXAFS) spectra (Figure 1e) displayed a main peak at 1.5 Å, corresponding to Cu–O bonds.¹ Moreover, no peaks attributed to metal Cu–Cu bonds were observed around 2.2 Å,⁹ indicating that Cu species are atomically distributed in CuSiO_x with extremely abundant atomic-level Cu–O–Si interfacial sites. The fitting results of EXAFS spectra (Figure S7 and Table S1) showed that the average coordination number (CN) of Cu–O bonds in CuSiO_x was 3.7, which was slightly lower than that of CuGeO₃ (CN_{Cu–O} = 4.03).

Electrochemical CO₂R Performance Evaluation. The electrochemical CO₂R activity and selectivity of the catalysts were first investigated in a three-electrode H-cell system. Compared with the Ar-saturated electrolyte, the catalysts gave higher current densities in the CO₂-saturated electrolyte, indicating that the CO₂R reaction occurred in the system (Figure 2a). As shown in Figure 2b, the main product of CO₂R with CuSiO_x was CH₄, with a maximum faradic efficiency (FE) of 72.5% at -1.27 V vs reversible hydrogen electrode (RHE, with iR correction) and a partial current density of -10.8 mA cm⁻² (Figures S8 and S9). Meanwhile, the FE of liquid and other gas products was significantly suppressed (Figure S11). Compared with other reported works, CuSiO_x showed significant CH₄ activity at lower overpotentials (Figure 2d). H₂ was the main CO₂R product for commercial CuO, and the highest FE_{CH₄} was 39.8% with the corresponding partial current density of only -1 mA cm⁻², which was much lower than that of CuSiO_x (Figures 2c and S9). For CuGeO₃, the CO₂R product is mainly H₂ with a small amount of CO, and no other gas-phase or liquid-phase products were detected, which might be ascribed to the excellent hydrogen evolution

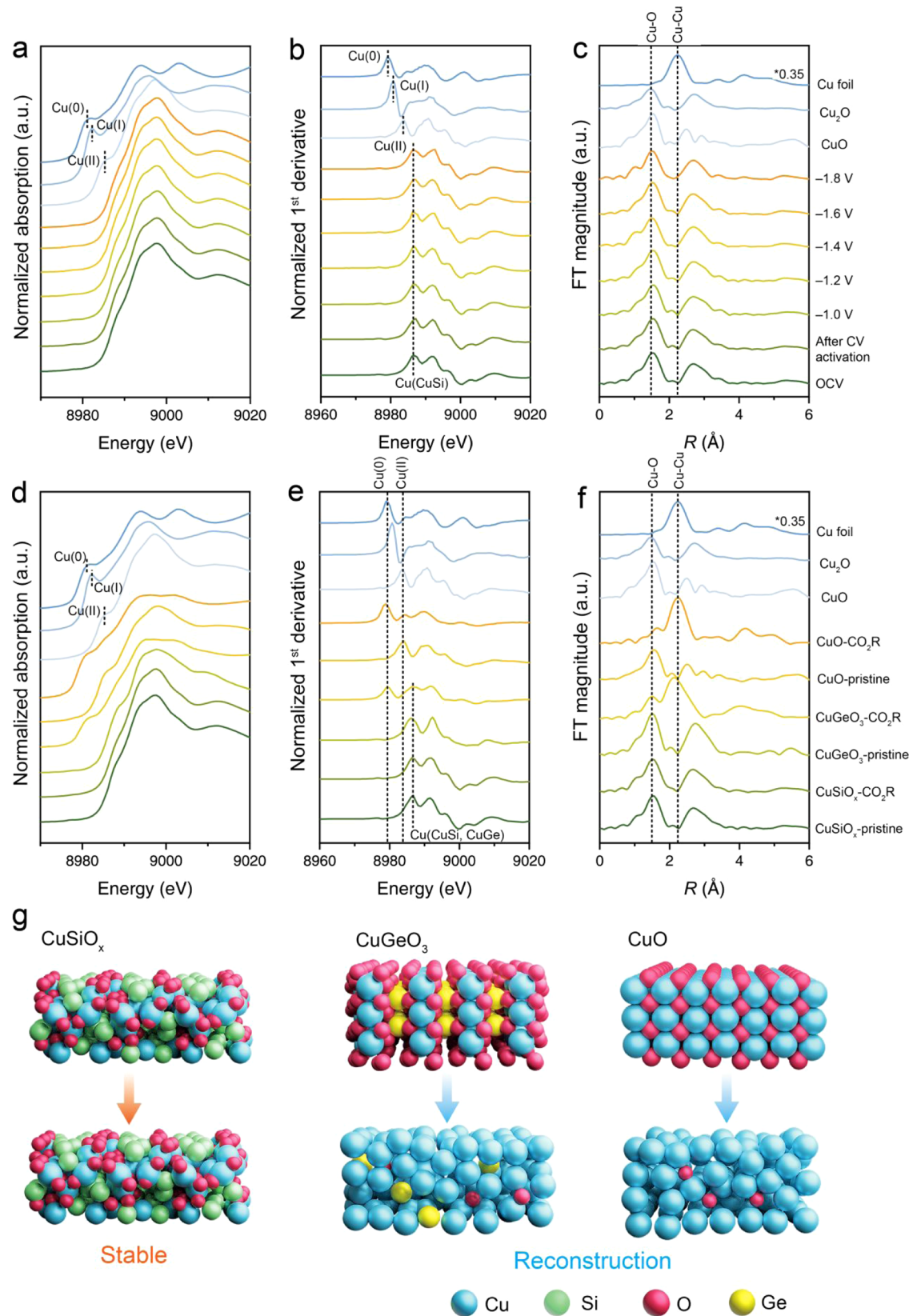


Figure 3. In situ XAS characterization. Potential dependence of *in situ* (a) Cu K-edge XANES spectra, (b) first-order derivatives of the XANES spectra, and (c) EXAFS spectra of the CuSiO_x under CO_2R using chronoamperometry (CA). *In situ* (d) Cu K-edge XANES spectra, (e) first-order derivatives of the XANES spectra, (f) EXAFS spectra, and (g) the corresponding schematic diagrams of structural evolution of CuSiO_x , CuGeO_3 , and CuO before and after CO_2R at -1.4 V vs RHE for 2 h.

reaction (HER) performance of metal Ge compounds (Figures S10 and S11).²⁶

In addition, we investigated the influence of different Cu contents on the electroreduction performance (Figure S12 and Table S2). As shown in Figure S13, CH_4 is the main product for all samples with different Cu contents, which may be attributed to the excellent electrochemical CO_2 methanation performance of Cu–O–Si interfacial sites. With increasing Cu content, the CH_4 selectivity showed a volcano plot, while the ethylene selectivity gradually increased. This suggests that the excess adjacent Cu sites in CuSiO_x may promote the C–C coupling process. As a comparison, we also synthesized $\text{CuO} + \text{SiO}_2$ catalyst by physical mixing. As shown in Figure S14a, the physically mixed sample showed an increased selectivity for CH_4 compared to commercial CuO, which may be attributed to the increased Cu–O–Si interfacial sites in $\text{CuO} + \text{SiO}_2$. However, its electrochemical stability is very poor; the FE_{CH_4} rapidly declines within 3 h (Figure S14b).

Benefiting from the excellent activity of CuSiO_x , we performed the long-term durability test at a constant potential of -1.6 V vs RHE for more than 12 h and found that FE_{CH_4} remains above 60%, which might be related to its excellent structural stability (Figure 2e). Furthermore, we tested the electrochemical CO_2R performance of CuSiO_x in 1 M KOH by a flow cell device (Figure S15), and the results showed that the CuSiO_x catalyst also exhibited excellent CO_2 -to- CH_4 activity in the potential range of -1.2 to -1.8 V ($j_{\text{total}} > 120 \text{ mA cm}^{-2}$, FE_{CH_4} around 50%), in which the highest j_{CH_4} reached $-170.4 \text{ mA cm}^{-2}$ at -1.6 V vs RHE , and the corresponding CO_2 -to- CH_4 conversion rate was as high as $0.22 \mu\text{mol cm}^{-2} \text{ s}^{-1}$, which exceeded most of the reported catalysts (Figure 2f and Table S3).

Furthermore, various characterizations were performed to unveil the structural stability of these catalysts after CO_2R . As shown in Figure S16a–c, the morphology of CuSiO_x was maintained after the CO_2R reaction, and no apparent structural reconstruction and metal Cu segregation occurred. EDS-mapping images also showed that Cu, Si, and O elements were still uniformly distributed in the nanotubes (Figure S16d). The XRD patterns of after- CO_2R CuSiO_x indicated no metallic Cu appeared (Figure S17a). On the contrary, the crystallinity of CuGeO_3 and CuO decreased or even completely disappeared after the reaction, accompanied by the appearance of metal Cu diffraction peaks, suggesting the structural reconstruction of these catalysts (Figure S17b,c). X-ray photoelectron spectroscopy (XPS) was used to characterize the electronic structure of the catalysts. The results suggested that the ratio of Cu^{2+} in CuSiO_x remains constant during the CO_2R process, whereas Cu^{2+} could not be stabilized, and almost all of them were reduced to Cu^0 in CuGeO_3 and CuO (Figure S17d–f). The ICP-OES (Table S2) and XPS semi-quantitative analysis (Table S4) results revealed no apparent change in the element content in CuSiO_x before and after the reaction, while the content of Ge in CuGeO_3 decreased significantly, resulting in structural damage. Similarly, the CuO species in $\text{CuO} + \text{SiO}_2$ also underwent almost complete reconstruction to form metallic Cu after CO_2R (Figure S18). It can be concluded that although physical mixing with SiO_2 can increase the Cu–O–Si interface to enhance the electrochemical activity of CuO, the interfacial interactions brought by this physical mixing were far inferior to the atomic Cu–O–Si interface in CuSiO_x and therefore could not increase the stability of the Cu–O species.

In Situ XAS Characterization. To investigate the oxidation state and structural evolutions of catalysts during the CO_2R process, we carried out *in situ* XAS studies (Figures 3a–f and S19–25). During the test, the working electrode potential was gradually decreased from the open-circuit voltage (OCV) to -1.8 V vs RHE , and each potential was held for at least 30 min to ensure that the catalyst reached an electrochemically stable state. Under the OCV conditions (Figure 3a,b), the peak at $\sim 8986 \text{ eV}$ ascribed to Cu(II) in CuSiO_x could be observed in the derivative curves of the Cu K-edge XNAES spectra, and the oxidation state did not change after CV activation. In the following tests, it was surprising to find that the Cu(II) peak at $\sim 8986 \text{ eV}$ was maintained over the potential range of -1.0 to -1.8 V vs RHE , and the Cu(0) and Cu(I) peaks at ~ 8979 and $\sim 8981 \text{ eV}$, respectively, were not detected,⁵⁰ indicating that the active Cu species in CuSiO_x were ultrastable during CO_2R process at different potentials, and no apparent reduction of Cu (II) occurs. Consistent with XANES results, EXAFS spectra showed (Figure 3c) that the Cu–O bond at $\sim 1.5 \text{ \AA}$ was maintained, and the Cu–Cu bond at $\sim 2.2 \text{ \AA}$ did not appear as the cathode potential decreased.^{1,9} It indicated that the active Cu species remain structural-stable and reconstruction-resistant over a broad potential window during the CO_2R process, which might attribute to the strong metal–support interaction in the atomic Cu–O–Si interfacial sites.

Furthermore, we performed long-term electrolysis experiments at -1.4 V vs RHE for 2 h to explore the structural stability of these three catalysts. As displayed in Figures 3d,e and S22, the Cu(II) species in CuSiO_x were preserved after long-time electrolysis, and no peaks corresponding to Cu(0) or Cu(I) appeared, showing ultrahigh stability. For CuGeO_3 , the Cu(II) peak intensity was significantly reduced after 2 h of electrolysis, and a distinct Cu(0) peak was observed at $\sim 8979 \text{ eV}$, indicating the reduction of Cu(II) to Cu(0). For commercial CuO, Cu(II) was almost completely reduced to Cu(0) after 2 h of electrolysis. The EXAFS spectra results show (Figures 3f and S23) that the Cu–O bonds at $\sim 1.5 \text{ \AA}$ in CuSiO_x have been stably maintained throughout the 2 h electrolysis process, without the formation of Cu–Cu bonds. The EXAFS fitting results (Figure S24 and Table S1) gave a Cu–O coordination number of 3.6, almost the same as one before the electrolysis, suggesting ultrahigh structural stability of atomic Cu–O–Si sites in the CO_2R reaction. However, the intensity of the peak corresponding to Cu–O bonds significantly vanished in CuGeO_3 and commercial CuO after 2 h of electrolysis, and a major peak ascribed to Cu–Cu bonds at $\sim 2.2 \text{ \AA}$ had appeared (Figure 3f), implying that the catalysts had undergone severe electrochemical reconstruction to generate metallic Cu particles. These structural evolutions can also be clearly observed from the wavelet transform (WT) spectra (Figure S25). The structure evolution schematic diagrams of the three catalysts during the electrochemical CO_2R process are summarized in Figure 3g. Combining the above *in situ* XAS results, it can be concluded that the atomic Cu–O–Si interfacial sites exhibited ultrahigh electrochemical stability and reconstruction resistance during the CO_2R process, which enabled the Cu species to maintain excellent catalytic performance over long-time electrolysis.

Theoretical Investigations by DFT Calculations. Density functional theory (DFT) and *ab initio* molecular dynamics (AIMD) calculations were used to further interpret the enhanced stability and excellent CO_2R performance of

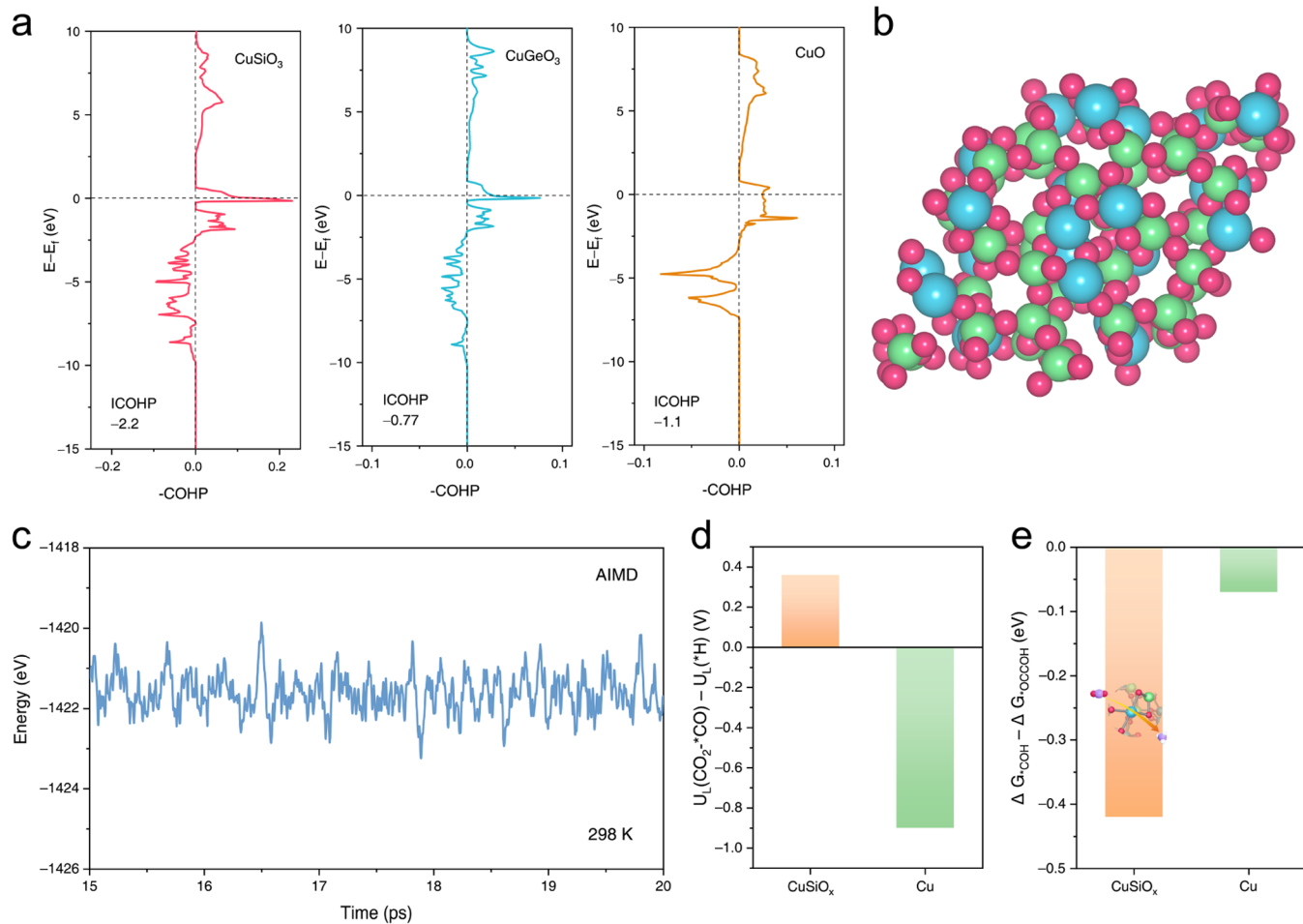


Figure 4. Theoretical simulation. (a) Projected crystal orbital Hamiltonian population (pCOHP) between the Cu center and O atom of CuSiO₃, CuGeO₃, and CuO. (b) Theoretical model of CuSiO_x. Blue, green, and red spheres represent copper, silicon, and oxygen atoms, respectively. (c) Total energy as a function of simulation time during the AIMD simulations. (d) Difference in limiting potentials for CO₂R and HER on CuSiO_x and Cu (111). (e) Reaction free energy difference between *CO protonation and C–C coupling steps on CuSiO_x and Cu (111) surfaces.

atomic Cu–O–Si interfacial sites. We first investigated the Cu–O bond strength of CuSiO₃, CuGeO₃, and CuO by the crystal orbital Hamilton populations (COHP). The order of energy-weighted ICOHP sums up to fermi level (E_f) was CuSiO₃ (-2.2 eV) < CuO (-1.1 eV) < CuGeO₃ (-0.77 eV) (Figure 4a). According to the ICOHP theory, the negative and positive values of ICOHP indicate bonding and antibonding interactions, respectively, and zero values refer to nonbonding interactions.⁵¹ The more negative the ICOHP value, the stronger the Cu–O bond strength. Compared with CuGeO₃ or CuO, silica can effectively improve the stability of Cu–O bond, thereby improving the electrochemical stability of Cu–O–Si interface sites during CO₂R process, which is consistent with the *in situ* XAS experiment results. Subsequently, we constructed the structural model of CuSiO_x according to the element ratios (Table S4) and performed AIMD simulations in the canonical ensemble (NVT) to optimize the structural model.⁵² As shown in Figure 4c, the system was followed by 20 ps of simulation with a time step of 2 fs to give the final stable CuSiO_x structure, in which each Cu atom was connected with 4 or 3 O atoms and formed an amorphous structure (Figures 4b and S26), which is consistent with the HRTEM and XAS results. It is worth mentioning that the system energy remains basically unchanged from 15 ps, indicating the excellent stability of the amorphous structure.

Moreover, the electrochemical CO₂R selectivity of CuSiO_x was also investigated by DFT simulations. We first calculated the thermodynamic limiting potential difference of CO₂R-to-*CO (* represents the adsorption site) and HER-to-*H ($U_L(\text{CO}_2\text{-*CO}) - U_L(\text{*H})$, a descriptor of the propensity for CO₂R vs HER).⁵³ It is generally accepted that a more positive $U_L(\text{CO}_2\text{-*CO}) - U_L(\text{*H})$ value corresponds to a better CO₂R selectivity in terms of reaction thermodynamics. We simulated all surface Cu sites of CuSiO_x and found that the $U_L(\text{CO}_2\text{-*CO})_{\min} - U_L(\text{*H})_{\min}$ value of CuSiO_x was more positive than that of metallic copper (the reconstructed product of CuO) (Figures 4d, S26, S27, and Table S5), suggesting that CuSiO_x has a better CO₂R selectivity compared to metallic copper, and the competing HER side reaction is suppressed. It is generally believed that the further protonation of adsorbed CO to *COH is a crucial step for CO₂ reduction to CH₄.^{54–57} We calculated the reaction free energy barrier diagram for CO₂ → *COOH → *CO → *COH on CuSiO_x and found that the path of *CO hydrogenation to *COH is quite beneficial in terms of thermodynamics, indicating that the formation of CH₄ on CuSiO_x is highly advantageous (Figure S28). In addition, we also considered the competitive relationship between the *CO hydrogenation to methane pathway and the C–C coupling pathway. It is widely assumed that the reaction free energy difference between *CO-to-*COH ($\Delta G_{*\text{COH}}$) and

*CO-to-*OCCOH (ΔG_{*OCCOH}) can serve as a descriptor of the propensity for CH_4 pathway vs C–C coupling.^{40,44,46} As shown in Figure 4e, we found that the $\Delta G_{*COH\text{min}} - \Delta G_{*OCCOH\text{min}}$ value of CuSiO_x was more negative than that of metallic copper, indicating that *CO protonation is energetically favorable on atomic Cu–O–Si interface sites compared to on Cu, thus promoting the CH_4 generation. In summary, DFT calculations suggested that the interface with silica could increase the Cu–O bond strength, thus improving the electrochemical stability and reconstruction resistance of Cu–O–Si interface sites. And the Cu–O–Si interface sites favor the production of methane through a pathway involving the *CO protonation to *COH instead of C–C coupling.

To demonstrate the high intrinsic activity of the Cu–O–Si interfacial sites for CH_4 , we destroyed the Cu–O–Si interface of CuSiO_x by heat treatment under air or hydrogen. The XRD patterns and XPS results (Figures S29 and S30) indicated that only part of the Cu–O–Si interfaces were destroyed and converted into CuO in CuSiO_x -air, whereas almost all Cu–O–Si interfacial sites were destroyed and aggregated into Cu particles in CuSiO_x -H₂. Electrochemical results (Figures S31 and S32) revealed a decrease in the FE_{CH_4} for CuSiO_x -air due to the destruction of a part of Cu–O–Si interfacial sites, while the selectivity of CuSiO_x -H₂ was overturned, and the $\text{FE}_{\text{CH}_4}/\text{FE}_{\text{C}_2\text{H}_4}$ ratio was reduced from 44 to 1 at most, confirming the significance of Cu–O–Si interfacial sites for the electrocatalytic CO_2R methanation. This is consistent with the theoretical calculation results.

SUMMARY

In conclusion, we proposed an efficient approach to stabilize Cu-based CO_2R electrocatalysts by constructing Cu–O–Si interfaces and synthesized a unique amorphous CuSiO_x catalyst with abundant atomic-level Cu–O–Si interfacial sites. The *in situ* XAS and electrochemical results revealed that the Cu–O–Si interfacial sites exhibit ultrahigh electrochemical stability and excellent electrocatalytic CO_2R methanation performance. Theoretical calculations further confirm that the strong interfacial interaction between Cu and silica could increase the Cu–O bond strength and improve the reconstruction resistance of Cu–O–Si interface sites. This finding provides an efficient avenue to address the stability issues of Cu-based CO_2R electrocatalysts and the design of new catalytic active sites.

ASSOCIATED CONTENT

Supporting Information

The Supporting Information is available free of charge at <https://pubs.acs.org/doi/10.1021/jacs.3c01638>.

Detailed experimental procedures, characterization methods, and extended figures and tables (PDF)

AUTHOR INFORMATION

Corresponding Author

Chen Chen – Engineering Research Center of Advanced Rare Earth Materials, Department of Chemistry, Tsinghua University, Beijing 100084, China; orcid.org/0000-0001-5902-3037; Email: cchen@mail.tsinghua.edu.cn

Authors

Xin Tan – Engineering Research Center of Advanced Rare Earth Materials, Department of Chemistry, Tsinghua

University, Beijing 100084, China; orcid.org/0000-0001-9707-672X

Kaiyan Sun – Engineering Research Center of Advanced Rare Earth Materials, Department of Chemistry, Tsinghua University, Beijing 100084, China

Zewen Zhuang – Engineering Research Center of Advanced Rare Earth Materials, Department of Chemistry, Tsinghua University, Beijing 100084, China; College of Materials Science and Engineering, Fuzhou University, Fuzhou 350108, China

Betao Hu – Qian Xuesen Laboratory of Space Technology, China Academy of Space Technology, Beijing 100094, China

Yu Zhang – Engineering Research Center of Advanced Rare Earth Materials, Department of Chemistry, Tsinghua University, Beijing 100084, China

Qinggang Liu – Dalian Institute of Chemical Physics, Chinese Academy of Sciences, Dalian 116023, China

Chang He – Engineering Research Center of Advanced Rare Earth Materials, Department of Chemistry, Tsinghua University, Beijing 100084, China

Zhiyuan Xu – Engineering Research Center of Advanced Rare Earth Materials, Department of Chemistry, Tsinghua University, Beijing 100084, China

Chang Chen – Engineering Research Center of Advanced Rare Earth Materials, Department of Chemistry, Tsinghua University, Beijing 100084, China

Hai Xiao – Engineering Research Center of Advanced Rare Earth Materials, Department of Chemistry, Tsinghua University, Beijing 100084, China; orcid.org/0000-0001-9399-1584

Complete contact information is available at: <https://pubs.acs.org/10.1021/jacs.3c01638>

Author Contributions

[†]X.T., K.S., and Z.Z. contributed equally to this work.

Funding

This work was supported by the National Key R&D Program of China (2021YFF0500503) and the National Natural Science Foundation of China (21925202, U22B2071, 22102081).

Notes

The authors declare no competing financial interest.

ACKNOWLEDGMENTS

The authors thank the BL11B station at the Shanghai Synchrotron Radiation Facility and the 1W1B stations at the Beijing Synchrotron Radiation Facility. The authors acknowledge the support of the Analysis Center of Tsinghua University for XPS measurements. The authors also thank Dr. Zong, R. from Tsinghua University Analysis Center for his help on the AC-HAADF-STEM characterization. The authors thank the Beijing PARATERA Tech CO., Ltd. for providing high performance computing resources that have contributed to the theoretical simulations in this work.

REFERENCES

- Jiao, J.; Lin, R.; Liu, S.; Cheong, W. C.; Zhang, C.; Chen, Z.; Pan, Y.; Tang, J.; Wu, K.; Hung, S. F.; Chen, H. M.; Zheng, L.; Lu, Q.; Yang, X.; Xu, B.; Xiao, H.; Li, J.; Wang, D.; Peng, Q.; Chen, C.; Li, Y. Copper atom-pair catalyst anchored on alloy nanowires for selective and efficient electrochemical reduction of CO_2 . *Nat. Chem.* 2019, 11, 222–228.

- (2) Gu, H.; Wu, J.; Zhang, L. Recent advances in the rational design of single-atom catalysts for electrochemical CO_2 reduction. *Nano Res.* **2022**, *15*, 9747–9763.
- (3) Li, F.; Thevenon, A.; Rosas-Hernandez, A.; Wang, Z.; Li, Y.; Gabardo, C. M.; Ozden, A.; Dinh, C. T.; Li, J.; Wang, Y.; Edwards, J. P.; Xu, Y.; McCallum, C.; Tao, L.; Liang, Z. Q.; Luo, M.; Wang, X.; Li, H.; O'Brien, C. P.; Tan, C. S.; Nam, D. H.; Quintero-Bermudez, R.; Zhuang, T. T.; Li, Y. C.; Han, Z.; Britt, R. D.; Sinton, D.; Agapie, T.; Peters, J. C.; Sargent, E. H. Molecular tuning of CO_2 -to-ethylene conversion. *Nature* **2020**, *577*, 509–513.
- (4) Yang, D.; Wang, G.; Wang, X. Photo- and thermo-coupled electrocatalysis in carbon dioxide and methane conversion. *Sci. China Mater.* **2019**, *62*, 1369–1373.
- (5) Ye, C.; Yu, X.; Li, W.; He, L.; Hao, G.; Lu, A. Engineering of Bifunctional Nickel Phosphide@Ni-N-C Catalysts for Selective Electroreduction of $\text{CO}_2\text{-H}_2\text{O}$ to Syngas. *Acta Phys. Chim. Sin.* **2022**, *38*, No. 2004054.
- (6) Liu, C.; Wu, Y.; Fang, J.; Yu, K.; Li, H.; He, W.; Cheong, W.-C.; Liu, S.; Chen, Z.; Dong, J.; Chen, C. Synergetic effect of nitrogen-doped carbon catalysts for high-efficiency electrochemical CO_2 reduction. *Chin. J. Catal.* **2022**, *43*, 1697–1702.
- (7) Gao, D.; Arán-Ais, R. M.; Jeon, H. S.; Roldan; Cuenya, B. Rational catalyst and electrolyte design for CO_2 electroreduction towards multicarbon products. *Nat. Catal.* **2019**, *2*, 198–210.
- (8) Ren, F.; Hu, W.; Wang, C.; Wang, P.; Li, W.; Wu, C.; Yao, Y.; Luo, W.; Zou, Z. An Extrinsic Faradaic Layer on CuSn for High-Performance Electrocatalytic CO_2 Reduction. *CCS Chem.* **2022**, *4*, 1610–1618.
- (9) Zhou, X.; Shan, J.; Chen, L.; Xia, B. Y.; Ling, T.; Duan, J.; Jiao, Y.; Zheng, Y.; Qiao, S. Z. Stabilizing Cu^{2+} Ions by Solid Solutions to Promote CO_2 Electroreduction to Methane. *J. Am. Chem. Soc.* **2022**, *144*, 2079–2084.
- (10) Birdja, Y. Y.; Pérez-Gallent, E.; Figueiredo, M. C.; Göttle, A. J.; Calle-Vallejo, F.; Koper, M. T. M. Advances and challenges in understanding the electrocatalytic conversion of carbon dioxide to fuels. *Nat. Energy* **2019**, *4*, 732–745.
- (11) Wang, P.; Yang, H.; Tang, C.; Wu, Y.; Zheng, Y.; Cheng, T.; Davey, K.; Huang, X.; Qiao, S. Z. Boosting electrocatalytic CO_2 -to-ethanol production via asymmetric C-C coupling. *Nat. Commun.* **2022**, *13*, No. 3754.
- (12) Popović, S.; Smiljanic, M.; Jovanovic, P.; Vavra, J.; Buonsanti, R.; Hodnik, N. Stability and Degradation Mechanisms of Copper-Based Catalysts for Electrochemical CO_2 Reduction. *Angew. Chem., Int. Ed.* **2020**, *59*, 14736–14746.
- (13) Kibria, M. G.; Dinh, C. T.; Seifitokaldani, A.; De Luna, P.; Burdyny, T.; Quintero-Bermudez, R.; Ross, M. B.; Bushuyev, O. S.; Garcia de Arquer, F. P.; Yang, P.; Sinton, D.; Sargent, E. H. A Surface Reconstruction Route to High Productivity and Selectivity in CO_2 Electroreduction toward C_{2+} Hydrocarbons. *Adv. Mater.* **2018**, *30*, No. 1804867.
- (14) Li, C. W.; Ciston, J.; Kanan, M. W. Electroreduction of carbon monoxide to liquid fuel on oxide-derived nanocrystalline copper. *Nature* **2014**, *508*, 504–507.
- (15) Verdaguer-Casadevall, A.; Li, C. W.; Johansson, T. P.; Scott, S. B.; McKeown, J. T.; Kumar, M.; Stephens, I. E.; Kanan, M. W.; Chorkendorff, I. Probing the Active Surface Sites for CO Reduction on Oxide-Derived Copper Electrocatalysts. *J. Am. Chem. Soc.* **2015**, *137*, 9808–9811.
- (16) Jeon, H. S.; Kunze, S.; Scholten, F.; Roldan Cuenya, B. Prism-Shaped Cu Nanocatalysts for Electrochemical CO_2 Reduction to Ethylene. *ACS Catal.* **2018**, *8*, 531–535.
- (17) Mistry, H.; Varela, A. S.; Bonifacio, C. S.; Zegkinoglou, I.; Sinev, I.; Choi, Y. W.; Kisslinger, K.; Stach, E. A.; Yang, J. C.; Strasser, P.; Cuenya, B. R. Highly selective plasma-activated copper catalysts for carbon dioxide reduction to ethylene. *Nat. Commun.* **2016**, *7*, No. 12123.
- (18) Handoko, A. D.; Ong, C. W.; Huang, Y.; Lee, Z. G.; Lin, L.; Panetti, G. B.; Yeo, B. S. Mechanistic Insights into the Selective Electroreduction of Carbon Dioxide to Ethylene on Cu_2O -Derived Copper Catalysts. *J. Phys. Chem. C* **2016**, *120*, 20058–20067.
- (19) Li, Y.; Cui, F.; Ross, M. B.; Kim, D.; Sun, Y.; Yang, P. Structure-Sensitive CO_2 Electroreduction to Hydrocarbons on Ultrathin 5-fold Twinned Copper Nanowires. *Nano Lett.* **2017**, *17*, 1312–1317.
- (20) Kim, J. Y.; Hong, D.; Lee, J. C.; Kim, H. G.; Lee, S.; Shin, S.; Kim, B.; Lee, H.; Kim, M.; Oh, J.; Lee, G. D.; Nam, D. H.; Joo, Y. C. Quasi-graphitic carbon shell-induced Cu confinement promotes electrocatalytic CO_2 reduction toward C_{2+} products. *Nat. Commun.* **2021**, *12*, No. 3765.
- (21) Lu, X. K.; Lu, B.; Li, H.; Lim, K.; Seitz, L. C. Stabilization of Undercoordinated Cu Sites in Strontium Copper Oxides for Enhanced Formation of C_{2+} Products in Electrochemical CO_2 Reduction. *ACS Catal.* **2022**, *12*, 6663–6671.
- (22) Liang, Z. Q.; Zhuang, T. T.; Seifitokaldani, A.; Li, J.; Huang, C. W.; Tan, C. S.; Li, Y.; De Luna, P.; Dinh, C. T.; Hu, Y.; Xiao, Q.; Hsieh, P. L.; Wang, Y.; Li, F.; Quintero-Bermudez, R.; Zhou, Y.; Chen, P.; Pang, Y.; Lo, S. C.; Chen, L. J.; Tan, H.; Xu, Z.; Zhao, S.; Sinton, D.; Sargent, E. H. Copper-on-nitride enhances the stable electrosynthesis of multi-carbon products from CO_2 . *Nat. Commun.* **2018**, *9*, No. 3828.
- (23) Sun, J.; Yu, J.; Ma, Q.; Meng, F.; Wei, X.; Sun, Y.; Tsubaki, N. Freezing copper as a noble metal-like catalyst for preliminary hydrogenation. *Sci. Adv.* **2018**, *4*, No. eaau3275.
- (24) Xu, C.; Chen, G.; Zhao, Y.; Liu, P.; Duan, X.; Gu, L.; Fu, G.; Yuan, Y.; Zheng, N. Interfacing with silica boosts the catalysis of copper. *Nat. Commun.* **2018**, *9*, No. 3367.
- (25) van Deelen, T. W.; Hernández Mejía, C.; de Jong, K. P. Control of metal-support interactions in heterogeneous catalysts to enhance activity and selectivity. *Nat. Catal.* **2019**, *2*, 955–970.
- (26) Chen, X.; Zhang, H.; Zhang, Y. Transition metal doped graphene-like germanium carbide: Screening of high performance electrocatalysts for oxygen reduction, oxygen evolution, or hydrogen evolution. *Colloids Surf., A* **2021**, *630*, No. 127628.
- (27) Chang, C. J.; Lin, S. C.; Chen, H. C.; Wang, J.; Zheng, K. J.; Zhu, Y.; Chen, H. M. Dynamic Reoxidation/Reduction-Driven Atomic Interdiffusion for Highly Selective CO_2 Reduction toward Methane. *J. Am. Chem. Soc.* **2020**, *142*, 12119–12132.
- (28) Lin, L.; Liu, T.; Xiao, J.; Li, H.; Wei, P.; Gao, D.; Nan, B.; Si, R.; Wang, G.; Bao, X. Enhancing CO_2 Electroreduction to Methane with a Cobalt Phthalocyanine and Zinc-Nitrogen-Carbon Tandem Catalyst. *Angew. Chem., Int. Ed.* **2020**, *59*, 22408–22413.
- (29) Chen, Z.; Gao, M.-R.; Zhang, Y.-Q.; Duan, N.; Fan, T.; Xiao, J.; Zhang, J.; Dong, Y.; Li, J.; Yi, X.; Luo, J.-L. Tuning local carbon active sites saturability of graphitic carbon nitride to boost CO_2 electroreduction towards CH_4 . *Nano Energy* **2020**, *73*, No. 104833.
- (30) Yuan, M.; Shi, G.; Xie, Y.; Du, L.; Fu, X.; Chen, X.; Xie, W.; Lu, T. B.; Wang, M. Constructing Cu-C Bond in Graphdiyne-Regulated Cu Single Atom Electrocatalyst for CO_2 Reduction to CH_4 . *Angew. Chem., Int. Ed.* **2022**, *61*, No. e202203569.
- (31) Huang, M.; Gong, S.; Wang, C.; Yang, Y.; Jiang, P.; Wang, P.; Hu, L.; Chen, Q. Lewis-Basic EDTA as a Highly Active Molecular Electrocatalyst for CO_2 Reduction to CH_4 . *Angew. Chem., Int. Ed.* **2021**, *60*, 23002–23009.
- (32) Yin, J.; Gao, Z.; Wei, F.; Liu, C.; Gong, J.; Li, J.; Li, W.; Xiao, L.; Wang, G.; Lu, J.; Zhuang, L. Customizable CO_2 Electroreduction to C_1 or C_{2+} Products through Cu_y/CeO_2 Interface Engineering. *ACS Catal.* **2022**, *12*, 1004–1011.
- (33) Shi, G.; Yu, L.; Ba, X.; Zhang, X.; Zhou, J.; Yu, Y. Copper nanoparticle interspersed MoS_2 nanoflowers with enhanced efficiency for CO_2 electrochemical reduction to fuel. *Dalton Trans.* **2017**, *46*, 10569–10577.
- (34) Deng, B.; Huang, M.; Li, K.; Zhao, X.; Geng, Q.; Chen, S.; Xie, H.; Dong, X.; Wang, H.; Dong, F. The Crystal Plane is not the Key Factor for CO_2 -to-Methane Electrosynthesis on Reconstructed Cu_2O Microparticles. *Angew. Chem., Int. Ed.* **2022**, *61*, No. e202114080.
- (35) Yang, F.; Chen, A.; Deng, P. L.; Zhou, Y.; Shahid, Z.; Liu, H.; Xia, B. Y. Highly efficient electroconversion of carbon dioxide into

- hydrocarbons by cathodized copper-organic frameworks. *Chem. Sci.* **2019**, *10*, 7975–7981.
- (36) Guan, A.; Chen, Z.; Quan, Y.; Peng, C.; Wang, Z.; Sham, T.-K.; Yang, C.; Ji, Y.; Qian, L.; Xu, X.; Zheng, G. Boosting CO₂ Electroreduction to CH₄ via Tuning Neighboring Single-Copper Sites. *ACS Energy Lett.* **2020**, *5*, 1044–1053.
- (37) Tan, X.; Yu, C.; Zhao, C.; Huang, H.; Yao, X.; Han, X.; Guo, W.; Cui, S.; Huang, H.; Qiu, J. Restructuring of Cu₂O to Cu₂O@Cu-Metal-Organic Frameworks for Selective Electrochemical Reduction of CO₂. *ACS Appl. Mater. Interfaces* **2019**, *11*, 9904–9910.
- (38) Wang, Y.; Chen, Z.; Han, P.; Du, Y.; Gu, Z.; Xu, X.; Zheng, G. Single-Atomic Cu with Multiple Oxygen Vacancies on Ceria for Electrocatalytic CO₂ Reduction to CH₄. *ACS Catal.* **2018**, *8*, 7113–7119.
- (39) De Gregorio, G. L.; Burdyny, T.; Lojudice, A.; Iyengar, P.; Smith, W. A.; Buonsanti, R. Facet-Dependent Selectivity of Cu Catalysts in Electrochemical CO₂ Reduction at Commercially Viable Current Densities. *ACS Catal.* **2020**, *10*, 4854–4862.
- (40) Hung, S. F.; Xu, A.; Wang, X.; Li, F.; Hsu, S. H.; Li, Y.; Wicks, J.; Cervantes, E. G.; Rasouli, A. S.; Li, Y. C.; Luo, M.; Nam, D. H.; Wang, N.; Peng, T.; Yan, Y.; Lee, G.; Sargent, E. H. A metal-supported single-atom catalytic site enables carbon dioxide hydrogenation. *Nat. Commun.* **2022**, *13*, No. 819.
- (41) Wang, Y. R.; Liu, M.; Gao, G. K.; Yang, Y. L.; Yang, R. X.; Ding, H. M.; Chen, Y.; Li, S. L.; Lan, Y. Q. Implanting Numerous Hydrogen-Bonding Networks in a Cu-Porphyrin-Based Nanosheet to Boost CH₄ Selectivity in Neutral-Media CO₂ Electroreduction. *Angew. Chem., Int. Ed.* **2021**, *60*, 21952–21958.
- (42) Sedighian Rasouli, A.; Wang, X.; Wicks, J.; Lee, G.; Peng, T.; Li, F.; McCallum, C.; Dinh, C.-T.; Ip, A. H.; Sinton, D.; Sargent, E. H. CO₂ Electroreduction to Methane at Production Rates Exceeding 100 mA/cm². *ACS Sustainable Chem. Eng.* **2020**, *8*, 14668–14673.
- (43) Chen, S.; Su, Y.; Deng, P.; Qi, R.; Zhu, J.; Chen, J.; Wang, Z.; Zhou, L.; Guo, X.; Xia, B. Y. Highly Selective Carbon Dioxide Electroreduction on Structure-Evolved Copper Perovskite Oxide toward Methane Production. *ACS Catal.* **2020**, *10*, 4640–4646.
- (44) Wang, X.; Ou, P.; Wicks, J.; Xie, Y.; Wang, Y.; Li, J.; Tam, J.; Ren, D.; Howe, J. Y.; Wang, Z.; Ozden, A.; Finfrock, Y. Z.; Xu, Y.; Li, Y.; Rasouli, A. S.; Bertens, K.; Ip, A. H.; Graetzel, M.; Sinton, D.; Sargent, E. H. Gold-in-copper at low *CO coverage enables efficient electromethanation of CO₂. *Nat. Commun.* **2021**, *12*, No. 3387.
- (45) Sedighian Rasouli, A.; Wang, X.; Wicks, J.; Dinh, C.-T.; Abed, J.; Wu, F.-Y.; Hung, S.-F.; Bertens, K.; Huang, J. E.; Sargent, E. H. Ga doping disrupts C-C coupling and promotes methane electro-production on CuAl catalysts. *Chem. Catal.* **2022**, *2*, 908–916.
- (46) Wang, X.; Xu, A.; Li, F.; Hung, S. F.; Nam, D. H.; Gabardo, C. M.; Wang, Z.; Xu, Y.; Ozden, A.; Rasouli, A. S.; Ip, A. H.; Sinton, D.; Sargent, E. H. Efficient Methane Electrosynthesis Enabled by Tuning Local CO₂ Availability. *J. Am. Chem. Soc.* **2020**, *142*, 3525–3531.
- (47) Zhang, T.; Verma, S.; Kim, S.; Fister, T. T.; Kenis, P. J. A.; Gewirth, A. A. Highly dispersed, single-site copper catalysts for the electroreduction of CO₂ to methane. *J. Electroanal. Chem.* **2020**, *875*, No. 113862.
- (48) Chen, S.; Wang, B.; Zhu, J.; Wang, L.; Ou, H.; Zhang, Z.; Liang, X.; Zheng, L.; Zhou, L.; Su, Y. Q.; Wang, D.; Li, Y. Lewis Acid Site-Promoted Single-Atomic Cu Catalyzes Electrochemical CO₂ Methanation. *Nano Lett.* **2021**, *21*, 7325–7331.
- (49) Li, Y.; Xu, A.; Lum, Y.; Wang, X.; Hung, S. F.; Chen, B.; Wang, Z.; Xu, Y.; Li, F.; Abed, J.; Huang, J. E.; Rasouli, A. S.; Wicks, J.; Sagar, L. K.; Peng, T.; Ip, A. H.; Sinton, D.; Jiang, H.; Li, C.; Sargent, E. H. Promoting CO₂ methanation via ligand-stabilized metal oxide clusters as hydrogen-donating motifs. *Nat. Commun.* **2020**, *11*, No. 6190.
- (50) Lin, S. C.; Chang, C. C.; Chiu, S. Y.; Pai, H. T.; Liao, T. Y.; Hsu, C. S.; Chiang, W. H.; Tsai, M. K.; Chen, H. M. Operando time-resolved X-ray absorption spectroscopy reveals the chemical nature enabling highly selective CO₂ reduction. *Nat. Commun.* **2020**, *11*, No. 3525.
- (51) Duan, X.; Li, P.; Zhou, D.; Wang, S.; Liu, H.; Wang, Z.; Zhang, X.; Yang, G.; Zhang, Z.; Tan, G.; Li, Y.; Xu, L.; Liu, W.; Xing, Z.; Kuang, Y.; Sun, X. Stabilizing single-atomic ruthenium by ferrous ion doped NiFe-LDH towards highly efficient and sustained water oxidation. *Chem. Eng. J.* **2022**, *446*, No. 136962.
- (52) Sun, K.; Wu, X.; Zhuang, Z.; Liu, L.; Fang, J.; Zeng, L.; Ma, J.; Liu, S.; Li, J.; Dai, R.; Tan, X.; Yu, K.; Liu, D.; Cheong, W. C.; Huang, A.; Liu, Y.; Pan, Y.; Xiao, H.; Chen, C. Interfacial water engineering boosts neutral water reduction. *Nat. Commun.* **2022**, *13*, No. 6260.
- (53) Sun, K.; Yu, K.; Fang, J.; Zhuang, Z.; Tan, X.; Wu, Y.; Zeng, L.; Zhuang, Z.; Pan, Y.; Chen, C. Nature-Inspired Design of Molybdenum-Selenium Dual-Single-Atom Electrocatalysts for CO₂ Reduction. *Adv. Mater.* **2022**, *34*, No. 2206478.
- (54) Wang, Z.; Yuan, Q.; Shan, J.; Jiang, Z.; Xu, P.; Hu, Y.; Zhou, J.; Wu, L.; Niu, Z.; Sun, J.; Cheng, T.; Goddard, W. A., 3rd Highly Selective Electrocatalytic Reduction of CO₂ into Methane on Cu-Bi Nanoalloys. *J. Phys. Chem. Lett.* **2020**, *11*, 7261–7266.
- (55) Peterson, A. A.; Abild-Pedersen, F.; Studt, F.; Rossmeisl, J.; Nørskov, J. K. How Copper Catalyzes the Electroreduction of Carbon Dioxide into Hydrocarbon Fuels. *Energy Environ. Sci.* **2010**, *3*, 1311–1315.
- (56) Peterson, A. A.; Nørskov, J. K. Activity Descriptors for CO₂ Electroreduction to Methane on Transition-Metal Catalysts. *J. Phys. Chem. Lett.* **2012**, *3*, 251–258.
- (57) Nie, X.; Esopi, M. R.; Janik, M. J.; Asthagiri, A. Selectivity of CO₂ reduction on copper electrodes: the role of the kinetics of elementary steps. *Angew. Chem., Int. Ed.* **2013**, *52*, 2459–2462.

□ Recommended by ACS

Enriching Reaction Intermediates in Multishell Structured Copper Catalysts for Boosted Propanol Electrosynthesis from Carbon Monoxide

Huitong Du, Wenlei Zhu, et al.

APRIL 17, 2023

ACS NANO

READ ▶

CeO₂/Cu₂O/Cu Tandem Interfaces for Efficient Water–Gas Shift Reaction Catalysis

Zhengjian Li, Guangxu Chen, et al.

JUNE 20, 2023

ACS APPLIED MATERIALS & INTERFACES

READ ▶

Interfacial Synergy between the Cu Atomic Layer and CeO₂ Promotes CO Electrocoupling to Acetate

Tang Yang, Xiaoqing Huang, et al.

APRIL 27, 2023

ACS NANO

READ ▶

Identifying an Interfacial Stabilizer for Regeneration-Free 300 h Electrochemical CO₂ Reduction to C₂ Products

Xinyu Wang, Yujie Xiong, et al.

DECEMBER 01, 2022

JOURNAL OF THE AMERICAN CHEMICAL SOCIETY

READ ▶

Get More Suggestions >